Possible electromagnetic disturbances causal by Spacecraft---Plasma Interactions at $4\,R_S$: Small Solar Probe

M . OKADA[1], B. T. TSURUTANI[2], B. E. GOLDSTEIN[2]

A. 1,. BRINCA[3], H. MATSUMOTO[1] and 1'. J. KELLOGG[4]

(November 24, 1993)

1

Abstract

The proposed Small Solar 1 'robe mission features a close approach to the sun with a perihelion of 4 R_s. Carbon molecules emitted from the spacecraft's heat shield will become ionized by electron impact and photoion ization. The newly created ions and electrons may generat e electromagnetic and electrostatic plasma waves between LF (1 of).) and VLF ($0.2\Omega_{C2+}$) which are possible sources of interference with in-situ plasma measurem ents. To understand this possible interference, we have performed computer simulations to model the electromagnetic and electrostatic field disturbances causal by the pick-up process of C_2^+ ions and related electrons as the spacecraft flies across the external

[1] 1 Radio At mospheric Science Cent er, Kyoto University, Uji, Kyot o 611, Japan

2 Jet Propulsion Laboratory, 4800 Oak Grove Drive, Padadena, CA 91109

3 Centro de Electrodinamica, Instituto Superior Tecnico, 1096 Lisbon Codex, Portugal

4 School of Physics and Astronomy, University of Minnesota, Minneapolis, MN

solar coron al magnetic field. in order t o study the wave particle interactions, which includes inhomogeneities (of the C_2^+) plasma) and kinetic effects, we use the electromagnetic particle code called Kyoto University Electromagnetic Particle Code (KEMPO) [*Matsumoto and Omura*, 1984]. We find that there arc no substantial plasma waves generated by the electron and ion pickup. The electric field near the spacecraft is also small. '1'1111s, there should be no interference for Small Solar l'robe. We will also give a first-principles argument why 1 ,ow Frequency instabilities should not occur.

1 Introduction

Knowledge about the solar corona, especially the region from 1 to 30 R_S, is quite limited. Plasma densities, temperatures and velocities are presently determined from remote optical and radio measurements, as well as by theoretical modeling. The observations and theory of the solar corona suggest the importance of coronal heating and acceleration in the outer portions of the corona, but the nature of this heating and acceleration is poorly understood at this time. Small Solar 1 'robe will be t he first spacecraft to measure the in situ plasma, magnetic field, plasma waves and energetic particle properties at $4R_s$. Other instruments to be carried on the spacecraft are an x-ray detector and a coronal imager. These near solar observations are the only way the processes that has't the upper corona and accelerated solar can make major progress.

The current Small Solar Probe mission design includes a carbon-carbon heat shield to protect the instruments from the intense solar radiation. Because the heat shield will reach up to 2100K at $4R_s$, C_2 neutral molecules will be evaporated into the solar wind. Present engineering designs are $dN_{C_2}/dt < 2.5$ mg s^{-1}. These carl)011 molecules

are then ionized by both solar radiation and electron impact ionization. The newly created ions and electrons are picked up by the solar wind plasma and magnetic field. In this process , the C_2-origin electrons will be accelerated by the Lorentz force ($\boldsymbol{v}_d \times \boldsymbol{B}$), where $\boldsymbol{v}_d$ is a velocity of the spacecraft relative to the solar wind ($\boldsymbol{v}_{sw}$ -- $\boldsymbol{v}_{sc}$). The newly created electrons may generate electron cyclotron harmonics in the high frequency regime, $f > \Omega_e$. The C_2^+ ions may be responsible for the generation of low frequency waves near the C_2^+ ion's cyclotron frequency. The purpose of this papper is to estima te the density modification in the vicinity of the spacecraft and the potential structure around the spacecraft (the spacecraft has been included in this modelling). We will also examine whether plasma instabilities occur and what wave amplitudes can be expected.

Interaction between the solar wind and heavy pickup ions has been t heoretically studid previously by many authors. *Golden et al.* [1973] have examined the stability condition for the beam- whistler, and for the beam- ion acoustic mode interactions in the limit m_e - → O. They suggest that unstable waves with zero group velocity in the spacecraft frame can exist near the leading edge of the shock for upstream Alfven Mach numbers greater than 5.5.

Brinca and Tsurutani [1989] analyzed the stability of low-frequency electromagnetic modes excited by coexisting newborn ions and showed that the effect of multiple ions on wave growth depends not only on their mass but also on the physical nature of the wave modes for given background magnetoplasma conditions and relative densities. Their stability analyses assured an isot ropic background and spatially uniform distribution of newborn ions.

Kojima et al. [1989], from numerical simulations, found a non-linear competing process for R-mode waves excited by water group ions near comets. *Omidi and Winske* [1 987] also examined the kinetic processes with solar wind mass loading due t o cometary

pickup ions. Although they took into account the density gradient near the cometary bow shock, they used hybrid simulation codes, which treat the electrons as a massless fluid, in order to analyze Low Frequency electromagnet ic modes.

Active experiments and spacecraft observations have been widely conducted for a decade. The Active Magnetospheric l'article 'J'racer Explorer (AMPTE) solar wind ion release mission provided information on the interaction between solar wind and the artificial ion cloud. *Gurnett et al.* [1986] reported shock-like electrostatic noise associated with the lithium ion release on September 11, 1984 and on September 20, 1984. They have presented detailed analysis of electrostatic instabilities for various lithum to proton density ratios. Two-dimensional structure around the lithum ion cloud is still not well understood. Applicability of their results to the small solar probe is also unclear.

Computer simulations are one of the most powerful methods to investigate spatial plasma inhomogeneities in the vicinity ofa spacecraft. In processes where wave particle interactions have a major role, a full-particle electromagnetic code is the appropriate method to use. We apply the KEMPO code to study the Small Solar Probe heat shield outgassing problem. In this paper we examine the spacecra ft environment at $4R_s$ with a full-particle simulation. We apply a realistic model, which takes into account the carbon outgassing at a rate of 2.5 mg s^{-1} (this is scaled in the computer simulations).

From a series of our computer simulations, we determine that the C_2 electrons diffuse very rapidly and are carried away from the spacecraft. On the contrary, the C_2^+ ions tend to stay close to the satellite. However, we should mention that the spacecraft environment is highly depend on the angle between the spacecraft velocity vector and the solar wind magnetic field. Our simulational results examine different angles of the solar wind magnetic field. We will discuss these results and will explain this dependence.

The contents of this paper arc as follows. First , we estimate C_2^+ density in the vicinity

of the spacecraft in Section 2. Then, we introduce the simulation model in Section 3. In Section 4, we present our results. We summarize and discuss t hese results in Section 5. We will also explain why LF wave generation is not expected in Section 5. Section 6 is the summary and describes the lack of C_2^+ and electron interference with the Small Solar Probe mission.

2 Density Estimation

First, we estimate the neutral C_2 density, ρ_{c2}, as a function of distance from the spacecraft, r. The neutral C_2 particles flow isotropically outward from the spacecraft. The density as a function of r is:

$$\rho_{c2} = \frac{Q}{4M_{C2}\pi r^2 V_n} \tag{1}$$

where Q is mass loss rate of the carbon heat shield in gm s^{-1}, M_{C2} is mass of C_2 ions in gm, r is the distance from the spacecraft in cm, and V_n is the out flow velocity of neutrals in cm s^{-1}. The ionization time of C_2 particles at $4R_S$ is assumed to be $\tau = 1.7 \times 10^{-2}$ sec^{-1} (*Goldstein* et, *al.* [1 990]). Assuming a spacecraft radius of 2 meters, an upper limit for the C_2^+ density is estimated assuming no removal by solar wind electric field (i.e., out flow of newly created ions with their initial velocity 1{,):

$$\rho_{C2+} = \int_{200}^{r} r^2 V_n \rho_{c2} \tau \, dr \tag{2}$$

An upper limit for Q is 2.5 x 10-0 gm s^{-1} and $V_n = 1.0 \times 10^5$ cm s^{-1} (*Goldstein et al* [1989]). The estimated pickup ion density is given in Figure 1. The maximum pickup ion density is about 1.3×10^4 cm^{-3} at a distance of 4×10^2 cm from the spacecraft surface. Fig.1

The solar wind parameters at the perihelion of Small Solar Probe, 4 solar radii from the center of the sun, are determined from solar parameters given in *Randolph* [1989].

The spacecraft velocity is 310 km s^{-1}. The nominal value of the magnetic field B_o at this distance may be taken as 0.1 Gauss; the solar wind plasma density N should be assumed to be 5×10^4 cm^3 The electron temperature T_e and ion temperatures T_i are taken to be 10^6K. The Alfven speed therefore is 2400 km s'1. The outward solar wind radial velocity V_{sw} of 400 km s^{-1} is parallel to the magnetic field. Using these parameters, the proton gyrofrequency Ω_p is 955 rad s^{-1}, the electron gyrofrequency Ω_e is 1.76 x 10^6 rad s^{-1}, the electron plasma frequency Π_e is 1.'26 x 10^7 rad s^{-1}, and the proton plasma frequency Π_p is 1.3 x 104 rad s-]. The proton inertial length, V_p/Ω_p is 1 km. The electron and proton Debye lengths are 0.5 m. The electric field in the spacecraft frame is 310 km s^{-1} x 0.1 Gauss = 3.1 V m^{-1}. The above solar wind parameters are summarized in Table 1. Table 1

In the Small Solar Probe mission, a heat shield is necessary to protect the scientific instruments. The instruments remain in the spacecraft umbra and are in an environment of 20°C. With the current spacecraft design, Figure 2, the heat shield consists of Carbon-Carbon material. Due to the extreme temperature of the heat shield at 4 R_s ($\sim$ '2100 K), some carbon molecules are evaporated by the strong solar irradiation. They are photoionized by solar UV and also created by electron impact ionization. The shield mass loss Q is required to be less than 2.5 mg s^{-1} at perihelion (Randolph [1991]). Instead of the neutral C_2 density given as equation (1), we use a Maxwellian distribution (with peak flux at the spacecraft surface) for ease of computation. This method overestimates the number of C_2 atoms at $r > R_o$ ($2R_o$ is the spacecraft dimension) and therefore is a worst-case situation. Fig.2

3 Model

A full-particle simulation code is used to study inhomogeneities in a solar wind spacecraft interaction. We first use 2-dimensional KEMPO code to solve for the electromagnetic and electrostatic fields and for particle trajectories. Maxwell's equations are solved by a leap-frog scheme for time advancement and a centered differential scheme is used for spatial differentiation. The equations of motion for particles are solved with a I\uncmall-1 Boris method (*Birdsall et al.* [1985]). In our simulation model (see Figure 3), a half open Fig.3 boundary condition is adopted. That is, damping regions are added in both x boundaries and periodic boundary conditions are used in the y dime.tioll. The plasma waves propagating in the x direction arc damped near the edges of the simulation box (see Figure 3) and particles are not traced beyond the $x = 0, x_{max}$ boundary. x_{max} represents the size of the system including the damping regions. At the center of the system we put in an internal boundary which corresponds to the spacecraft. This is indicated by the shaded box of size $2R_o$. In this model all particles impinging upon the spacecraft surface arc absorbed, that is, the reflection coefficient of the particles at the spacecraft surface is assumed to be zero. The potential of the spacecraft is calculated from the accumulated charge using a capacitance matrix method [*Hockney and Eastwood*, 1988]. The solar wind flows along x axis from left-to-right and the solar wind magnetic field has an angle 6' relative to the flow direction and lies within the $x - y$ plane. We choose the spacecraft as our frame of reference. The external electric field has an intensity of $- V_d \times B_o$. This is in the $- z$ direction, e.g., into the paper. In order to simulate an open boundary system, the solar wind particles are injected from both ends (because of the large thermal velocities, some particles enter the box from the right side), $x = 0, x_{max}$, with a constant ambient flux which is calculated from the thermal velocity and the solar

wind velocity V_{sw}. 'J'able 2

Table 2 gives the mode] paramcters. We find the electron beta, ion sound Mach number and Alfvén mach number are 0.013, 5.0 and 0.4, respectively. Note that the flow speed is supersonic but not super-Alfvénic. The characteristic frequencies of each species are chosen to maintain realistic ratios relative to the electron cyclotron frequency. The drift, ion thermal and ion sound velocities are indicated with a value normalized to the solar wind electron thermal velocity. Solar wind electrons and ions are considered to be isothermal. The mass ratios of the electrons, protons and C_2 ions are assured to be 1:16:100 in our simulation. The compressed mass ratio is necessary for resons of computational efficiency. The thermal velocity of C_2-origin electrons is assumed to be 10 times smaller than that of solar wind electrons. The thermal velocity of C_2 ions is very small, and therefore the ions can be assumed to be a cold beam in the solar wind. Figure 4 shows the velocity distribution] function used in the computer simulations. Fig.4

4 Results

We perform 4 computer simulation runs wit h different values of the angle of the external magnetic field relative to the solar wind flow direction and C_2 densities. Paramcters for each simulation run are listed in Table 3. We first perform a computer simulation without C_2 particles (θ = 30°) to identify what kind of waves are generated due to the spacecraft-solar wind interaction without pickup ions present. We do this for baseline information. Next we put the C_2 pickup plasma into the system and compare the difference between two cases at three different θ values (θ = 0°, 30° and 900). Fig.5

Figure 5 depicts the time evolution of (a) total energy, (b) electric field, (c) magnetic field, (d) the numb er of solar wind electrons, (e) the numb er of solar wind protons, (f)

the number of C_2-origin electrons, (g) the number of C_2^+ ions and (h) total number of particles, respectively. The simulation system reaches a steady state at time $\Omega_c t \simeq 300.0$. The total time of the simulation run is $\Omega_c t = 655.4$. This simulation time corresponds to the one C_2^+ gyroperiods. The frequency resolution is Ω_{c2+}. Thus, the system reaches steady state in $\sim 0.4\,\Omega_{c2+}$. Fig.6

Figure G shows the solar wind electron (a) and proton (b) density profiles at time $\Omega_c t = 655.4$ when the C_2 ions are not present. The density contour level is normalized by the solar wind undisturbed density n_o. A very small wake region develops behind the spacecraft, but no shock nor density enhancement occur. Fig.7

The next 3 cases (Figures '7, 8 and 9) illustrate the densities when C_2 ions are present. Figure 7 is the case where the external magnetic field has an angle of 0° relative to the solar wind flow direction. The density profiles of the solar wind electrons (a), protons (b), C_2-origin electrons (c) and C_2^+ ions (d) are shown, respectively. A solar wind ion wake is formed behind the spacecraft (see panel (b)). This is primarily caused by the C_2 ion density enhancement near the spacecraft (shown in panel (d)), displacing the solar wind protons. There is a C_2 ion density buildup in the vicinity of the spacecraft (panel (d)). The largest densities are on the upstream side of the spacecraft. While the newly created C_2^+ ions are removed slowly from the vicinity of the spacecraft, the C_2-origin electrons are carried away very fast by interacting with the solar wind electrons. Diffusion is the main reason for the rapid removal of the C_2^+ -origin electrons. The charge separation of the C_2^+ ions from the C_2-origin electrons creates an electric field in the vicinity of the spacecraft. This electric field pushes the C_2^+ ions in upstream direction. The Potential structure in the vicinity of the spacecraft will be shown in Figure 1 ().

There is also a small region of downstream density enhancement just behind the spacecraft. The cause of this enhancement is the focusing effect (*Al'pert* [1990]). Fig.8

As the the angle of the magnetic field relative to the spacecraft velocity increases (Figures 8 and 9), more C_2 electrons are carried away from the spacecraft. The C_2 ions again build up on the upstream side of the spacecraft. For the $\theta = 30°$ case, the absolute densities are almost the same as the $\theta == 0°$ case, but the C_2^+ ion density structure is now much broader in angle. This is because the C_2^+ ions can flow along the magnetic field and are accelerated by the solar wind electric field (note the asymmetry in the y direction). There is also again a high-density, narrow downstream enhancement region. Fig.9

Figure 9 represents the solar wind and C_2 plasma density with the same format as the previous Figure but for $\theta = 90°$. Because of the orthogonal field orientation, the C_2^+ density enhancement in the upstream region is now symmetric about the y direction. There is also now a lack of an enhancement in the downstream region. Fig.10

Figure 10 depicts the potential structure around the spacecraft with a bird's eye view for the $\theta = 90°$ case. A potential hill due to charge separation exists behind the spacecraft. The potential of the spacecraft itself is not affected much by spacecraft charging effects. The potential at spacecraft surface is almost 4 times the electron thermal energy ($\kappa_B T_e$). The corresponding electric field is $\sim 2.0 \times 10^{-19}\,\mathrm{V\,m^{-1}}$, a very low value. This potential is caused by the C_2^+ ions in the vicinity of the spacecraft. The maximum of this potential kept low due to the presence of background thermal electrons. The maximum of this potential is $\sim 4\kappa_B T_e \sim 5.6 \times 10^{-12} erg$. The drift energy of the solar wind proton is $\sim 7.5 \times 10^{-10} erg$. Thus, this should not lead to any interference with solar wind plasma detection.

Figures 11 and 12 show the wave spectra along the x axis at $y/\lambda_D = 17.0$ (panel (a)) and 25.2(panel (b)), respectively. Figure 11 shows the wave spectra when the C_2^+ plasma is present. On the other hand, Figure 12 corresponds to the case when the C_2^+ Fig.11 Fig.12

ions are not present. We cannot see any kind of wave generation in the vicinity of the spacecraft due to the C_2^+ plasma.

5 Instabilities

In this Section, we will consider two basic plasma instabilities related to Low Frequency (MHD) waves which may occur in the vicinity of the spacecraft. One is a resonant instability and the other a nonresonant instability.

5.1 Resonant Instabilities

We first consider the resonant case. Below is the condition for resonance between electromagnetic waves and ring-beam ions.

$$\omega - \boldsymbol{k} \cdot \boldsymbol{v} = n\Omega_{c2+} \tag{3}$$

where w is the Wave frequency, $\boldsymbol{k}$ the wave vector. $\boldsymbol{v}$ the velocity of the ion, and n is an integer 0, 1, ±2,... . For simplicity, we only will discuss the first order resonances (n = --1 for right-hand modes). in the resonant ion-beam case, the heat shield ions overtake right-hand waves. Through an anomalous Doppler shift, the ions sense the waves as left-handed (the same sense of rotation as the ion gyration about $\boldsymbol{B}$), and resonance occurs when:

$$\frac{V_{\|}}{V_{ph}} = 1 + \frac{\Omega_{c2+}}{\omega} \tag{4}$$

From the above expression it can be noted that there cannot be a resonant interaction if the particle parallel (along $\boldsymbol{B}$)velocity is less than the wave phase speed. From the previously given numbers, the particle velocity is 330 km s^{-1} relative to the solar wind plasma and the Alfven speed is 1200 km s^{-1}. Therefore, no waves are generated by this interaction.

5.2 Nonresonant Instabilities

For nonresonant instabilities, the ion beam densities must be $\geq 1\%$ of the ambient plasma density and/or the beam velocity ≥ 10 to 15 times the wave phase velocity (*Winske and Gary* 1986). We have already discussed the later and have noted that $V_{beam} << V_{ph}$, thus this condition is not met. The Small Solar Probe heat shield design is for a maximum outgassing of neutrals of 2.5 mg s^{-1}. Obviously for distances further than $4R_s$, the temperature and outgassing will be considerably less. Using the above numbers and the neutral velocity of 1 km s^{-1}, we get, a production rate of I ()' ions cm^{-3} s^{-1} at 3 km, the C_2^+ ion gyroradius. in the θ =- 90° case, t hese ions are rapidly swept away by the solar wind plasma at the velocity of 310 km s-" ^{1}. The " beam" density is thus over 4 orders of magnitude less than the solar wind density of 2 x 1 0^5 cm^{-3}. Because neither of the two requirements are met for the nonresonant instal bility, we would expect no wave generation from this mechanism.

6 Summary

We have performed 4 computer simulations, one without C_2 ions and others with C_2 ions and θ =- 0°, 30° and 90°.

There is an upstream C_2^+ density feature for all cases of O. The density enhancement has a magnitude of $\sim 4n_o$. This density enhancement is caused by the charge separation of C_2^+ ions and electrons. This spatial structure is commonly seen for all cases of U. The shape of this density feature is depend on 0. This is due to the v_{sw} x B drift of the ions. There is negligiblic potential near the spacecraft on the solar side. There is a small C_2^+ density wake behind the spacecraft for all cases except when θ = 90°. The density is again $\sim 2n_o$. The causes of this is a focusing effect. 'J here is a measureable spacecraft

potential but quite small $\sim$ 2.0 x 10- ^{19} V m^{-1}. We also compared the peak energy **of** the potential structure with the drift energy of the solar wind protons. We con firmed that the solar wind flow is not affected by this potential.

We also checked the wave intensity in the vicinity of t he spacecraft. We could not find any change in the frequency spectrum due to the C_2^+ plasma.

References

[1] Al'pert, Y. I,., Space plasma, Cambridge Univ. Press, 1990

[2] Birdsall, C. K. and A . B. Langdon, Plasma physics via computer simulation, *MacGra w-Hill*, 1985

[3] Brinca, A. I,. and B. T. Tsurutani, Influence of multiple ion species on low-frequency electromagnetic wave instabilities, *J. Geophys. Res.*, 94, 13565, 1989.

[4] Chen, F. F., Introduction to plasma physics., *Plenum Press, 249-256, 1974*

[5] Golden, 1<.1,1,. M. Linson and S. A. Mani, Ion streaming instabilities with apppli-cation to collisionless shock wave structure *Phys. of Fluids, 16, 2319,* 1973

[G] Goldstein, B. E., W. C. Feldman, 11.11. Garrett, I. Katz, L. Linson, K. W. Ogilvie, F. 1,. Scarf and E. C. Whipple, Spacecraft mass loss and electric potential requirements for the starprobe mission, J]'], 715-1 ()(), 1980

[7] Gurnett, D. A., T. Z. Ma, R. R. Anderson, 0. H. Bauer, G. Haerendel, B. Hausler, G. Paschmann, R. A. Treumann, H. C. Koons, R. Holzworth and H. Luhr, Analysis and interpretat ion of the shocklike electros tatic noise observed during the A MPTE solar wind lithium releases, *J. Geophys. Res.*, 91, 1301, 1986.

[8] Hockney, R. W., J. W. Eastwood, Computer simulation using particles, *Adam Hilger, Bristol and Philadelphia*, 1988

[9] Kojima, H, H. Matsumoto, Y. Omura and B. 'J'. Tsurutani, Nonlinear evolution of high frequency r-mode waves excited by water group ions near comets: computer experiments, *Geophys. Res. Lett.*, 1 G, 9-12, 1989.

[1O] Matsumoto, 11., K. Inagaki and Y. Omura, Computer simulation of passage of an electron beam through a plasma, *Adv. Space. Res.*, 8, pp. 1 51-160, *(1988).*

[11] Matsumoto, H. and Y. Omura, Particle simulation of electromagnetic waves and its application to space plasmas, *Computer Simulation of Space Plasmas*, 11. Matsumoto and T. Sat o, pp.43-1 02, Terra Scientific Publishing Company, (1 984).

[12] Matsumoto, }1., Coherent nonlinear effects on electromagnetic wave-l)article interactions, *Space Science Reviews*, 4 2 , pp.429- 448, D. Reidel Publishing Company, (1985).

[13] Omidi, N. and D. Winske, A kinetic study of solar wind mass loading and cometary bow shocks, *J. Geophys. Res.*, **92**, 13409, 1987.

[14] Omura, Y ., and I J. Matsumoto, Computer experiments on whistler and plasma wave emission for space lab-2 elect ron beam", *Geophys.* lies. *Lett.*, **15**, 319-322, 1988.

[15] Parker, E. N., Heating solar coronal holes, *Astrophys. J.*, 372, 719, 1991

[16] Parks, G. K., Physics of space plasmas, *AddisonWesley*, 204, 1 991

[17] Randolph, J. E., Solar Probe: Mission and system design concepts 1991, *JPL/CIT*, JPL D-8927, 1991

[18] Randolph, J. E., Solar Probe: Scientific rationale an mission concept, *JPL/CIT*, JPL *1)-6797, 1989*

[19] Tsurutani, B. 'J'., COMETS: A laboratory for plasma waves and instabilities, *AGU*, Geophysical Monograph 61, 1991

[20] Umeki, 11. and 'J'. Terasawa, Decay instability of in incoherent Alfvén waves in the solar wind, *J. Geophys. Res.*, *97,* 3113, 1992.

[21] Winske, *]),* and S. P. Gary, Electron agnetic inst abilit ies driven by cool heavy ion beam, *J. Geophys. Res.*, 91, 6825, 1986.

Acknowledgmensts

1 'ortions of this research were done at the Jet 1 'ropulsion Laborat ory, California Institute of Technology u nder contract with NASA. MO thanks Jet Propulsion Laboratory for their hospitality during his stay in 1991-2. BTT thanks RASC, Kyot o University for hosting him during portions of the writing of this paper. We would like to thank H. Kojima Of RASC for helpful scientific discussions.

Parameters		Value
Density	?/o(cIll- 3,	$2" 10^5$
Ambient B field	B_o(Gauss)	0.1
Electron Thermal Velocity	V_e((’111 s-^{1})	5.6”108
Proton Thermal Velocity	V_i(cm s^{-1})	1.3” 107
Electron Gyrofrequency	$\Omega_e/2\pi$(Hz)	$1.76.\ 10^6$
Proton Gyrofrequency	$\Omega_i/2\pi$(Hz)	960
Electron Larmor Radius	ρ_e(cm)	3.8.102
Proton Larmor Radius	ρ_i(cm)	1.4.104
Electron Plasma Frequency	$\Pi_e/2\pi$(Hz)	$25 \cdot 10^6$
Proton Plasma Frequency	$\Pi_i/2\pi$(Hz)	$5.9 \cdot 10^5$
Debye Length	λ_D(cm)	22.()
Alfvén Velocity	V_A(cm s^{-})	$1.2 \cdot 10^8$
Alfvén Mach Number	M_A	0.3
Ion Sound Velocity	V_s(cm s^{-1})	154.105
Sound Mach Number	M_s	2.()
C_2 ionization rate	7 (sec^{-1})	0.017

Table 1: Basic Parameters of the Solar Wind at $4R_s$

Parameters		
Electron Plasma Freq.	Π_e/Ω_e	4.0
Proton Cyclotron Freq.	Ω_p/Ω_e	1.0
Proton Plasma Freq.	Π_p/Ω_e	1.0
Proton Thermal Velocity	V_p/V_e	0.1
C_2^+ Cyclotron Freq.	Ω_{c2+}/Ω_e	0.04
C_2^+ Plasma Freq.	Π_{c2+}/Ω_e	0.01
C_2^+ Thermal Velocity	V_{c2+}/V_e	0.001
Mass ratio	$m_{C2} : m_p : m_e$	100:16:1
Debye length	λ_D	0.25
Spacecraft Size	R_o/λ_D	1.6
Alfvén Velocity	V_A/V_e	1.25
Electron Beta	β_e	0.013
Plasma Drift Velocity	V_d/V_e	0.5
Light Speed	c/V_e	10
Ion Sound Speed	V_s/V_e	0.1
Sound Mach Number	M_s	5.0
Alfvén Mach Number	M_A	0.4
Spatial grid	Δr	0.2
Time grid	Δr	0.01
Normalization Values		
Electron Cyclotron Freq.	Ω_e	1.0
Solar Wind Electron Thermal Velocity	V_e	1.0

Table 2: Normalized parameters used in the computer experiments. Normalizations are taken with respect to the electron cyclotron frequency, Ω_e, the solar wind electron thermal velocity, V_e.

Case No.	Fig. No.	θ^o	relative C_2 flux
(1)	6	30.0	0.0
(2)	7	0.0	4.0
(3)	8	30.0	4.0
(4)	5, 9, 10	90.0	4.0

Table 3: Parameters used in the simulation runs. C_2 number flux is defined relative to the solar wind particle number flux.

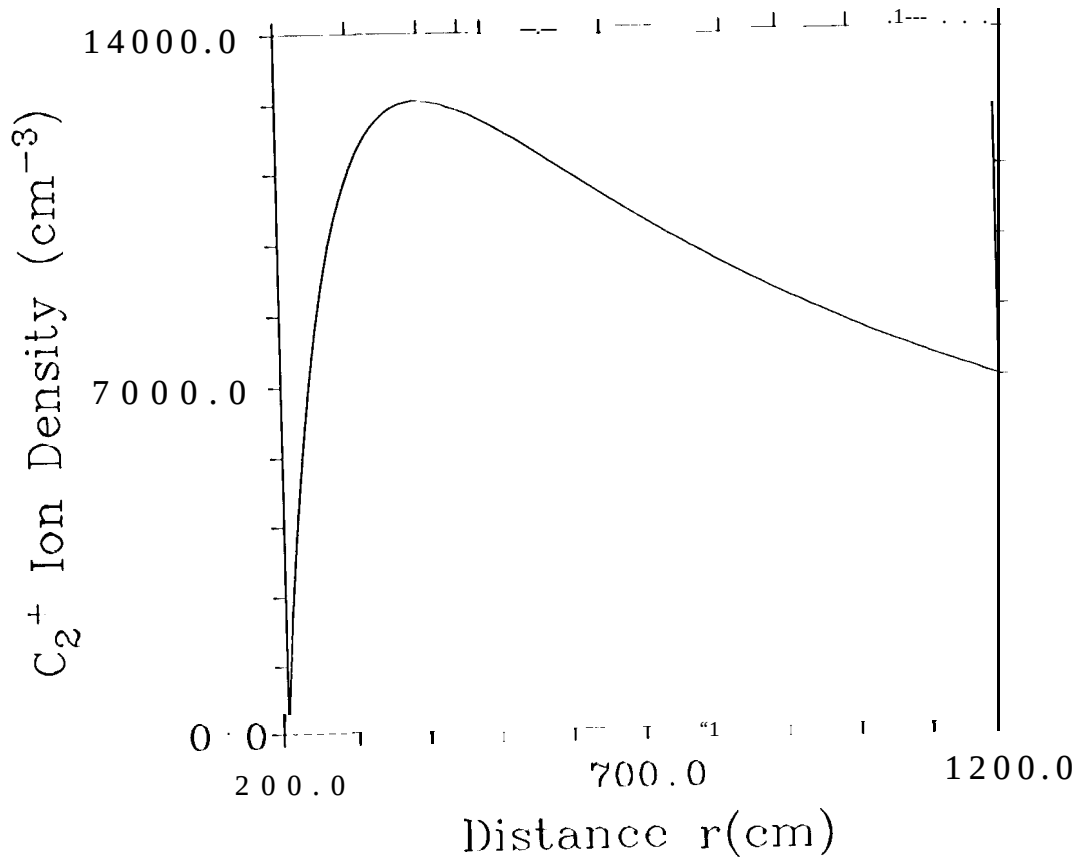

Figure 1: Estimated ion density ignoring solar wind electric fields as a function of distance r obtained from Eq. *(2)*. Maximum pickup ion density is about $1.3 \times 10^4\ cm^{-3}$ at a distance of 4 m from the spacecraf surface.

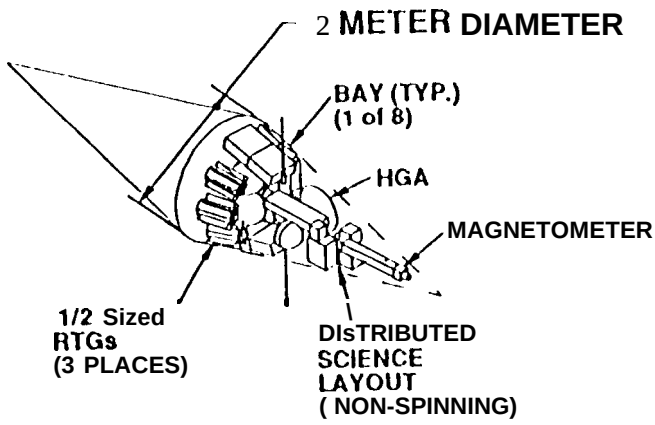

Figure 2: Small Solar Probe Spacecraft Configuration

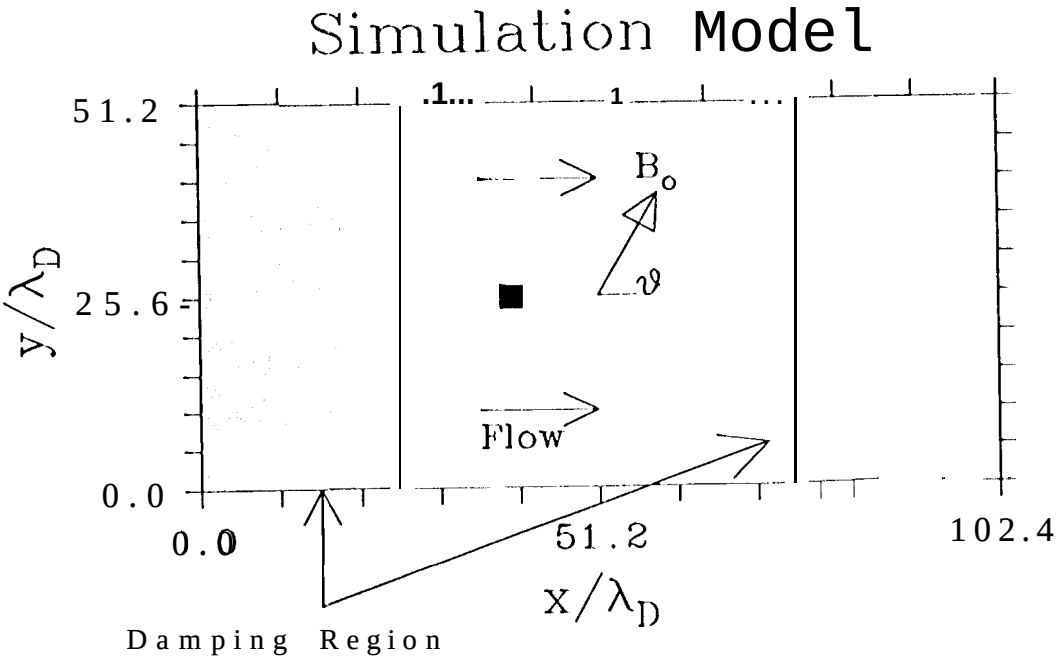

Figure 3: 2-dimensional computer simulation model. Damping region is attached at both ends of the x direction boundary. Periodic boundary condition has been adopted in y direction boundary. Internal boundary, which corresponds to the spacecraft, is located at the center of the physical region.

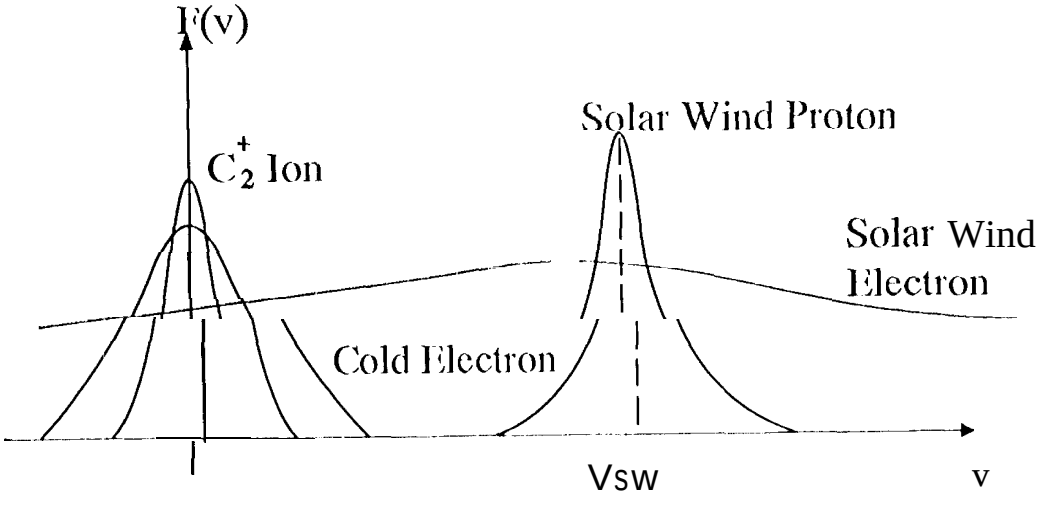

Figure **i:** Schematic velocity distributions of the four plasma populations in the simulation rnns. Hot solar wind electrons and p rot ons flow with a velocity V_{sw}. Photoion ized C_2 plasma has small thermal speed and no **no\\"** velocity on the spacecraft frame 01 1'('('('1'('11('('.

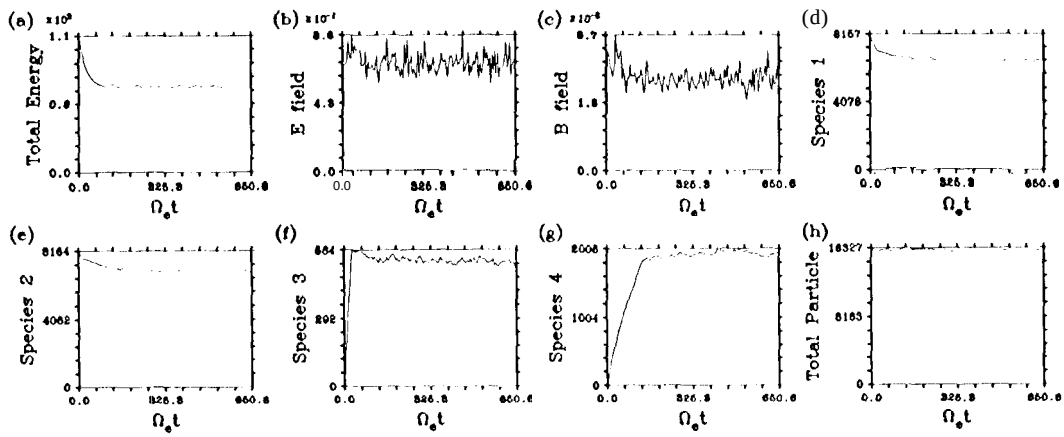

Figure 5: Energy and particle number evolution during simulation (4) of Table 3. The simulation system reaches the steady state at time $\Omega_e t \sim 300$." The figures show: (a) Total energy in the system, (b) Electric field energy, (c) Magnetic field energy, (d) Number of the solar wind electrons, (e) Number of the solar wind protons, (f) Number of the C_2 origin electrons and (g) Number of the C_2^+ ions, respectively. Energy is normalized by the solar wind electron kinetic energy, κT_e. Decrease of the total energy is due to outgoing energy flux of the solar wind electrons and ions, which is initially loaded in the simulation system. On the contrary the number of cold C_2^+ ion increases in time.

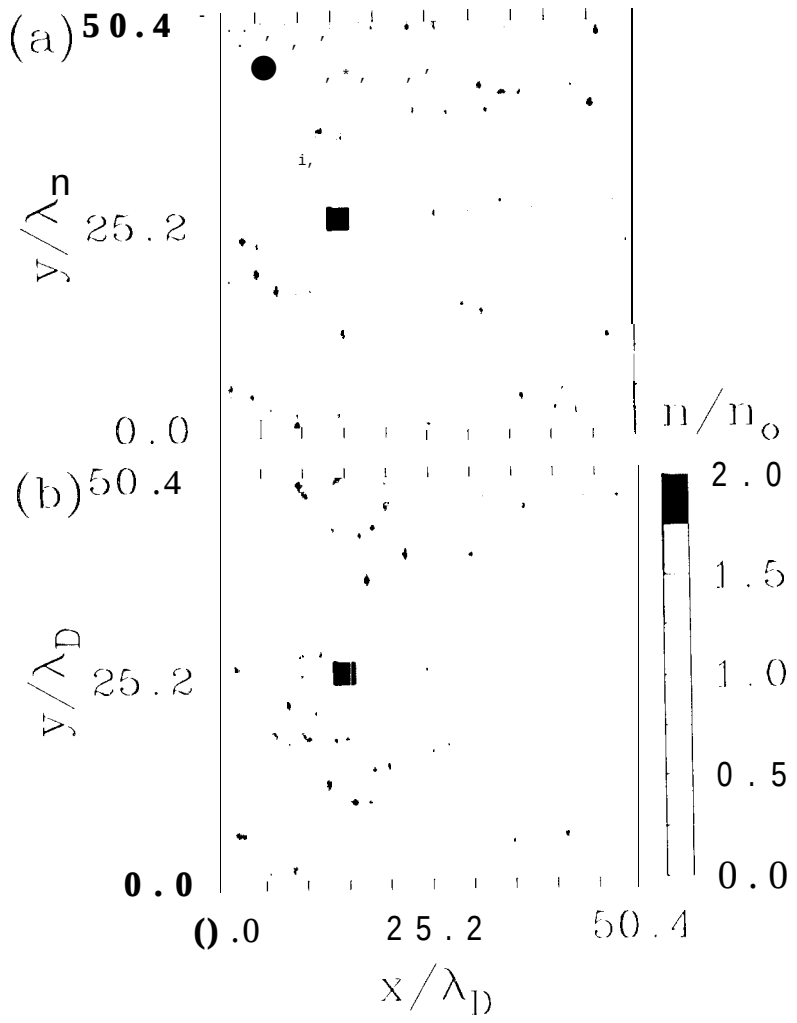

Figure 6: The solar wind electron (a) and proton (b) density profiles for the case $\theta = 30^o$ without C_2 particles.

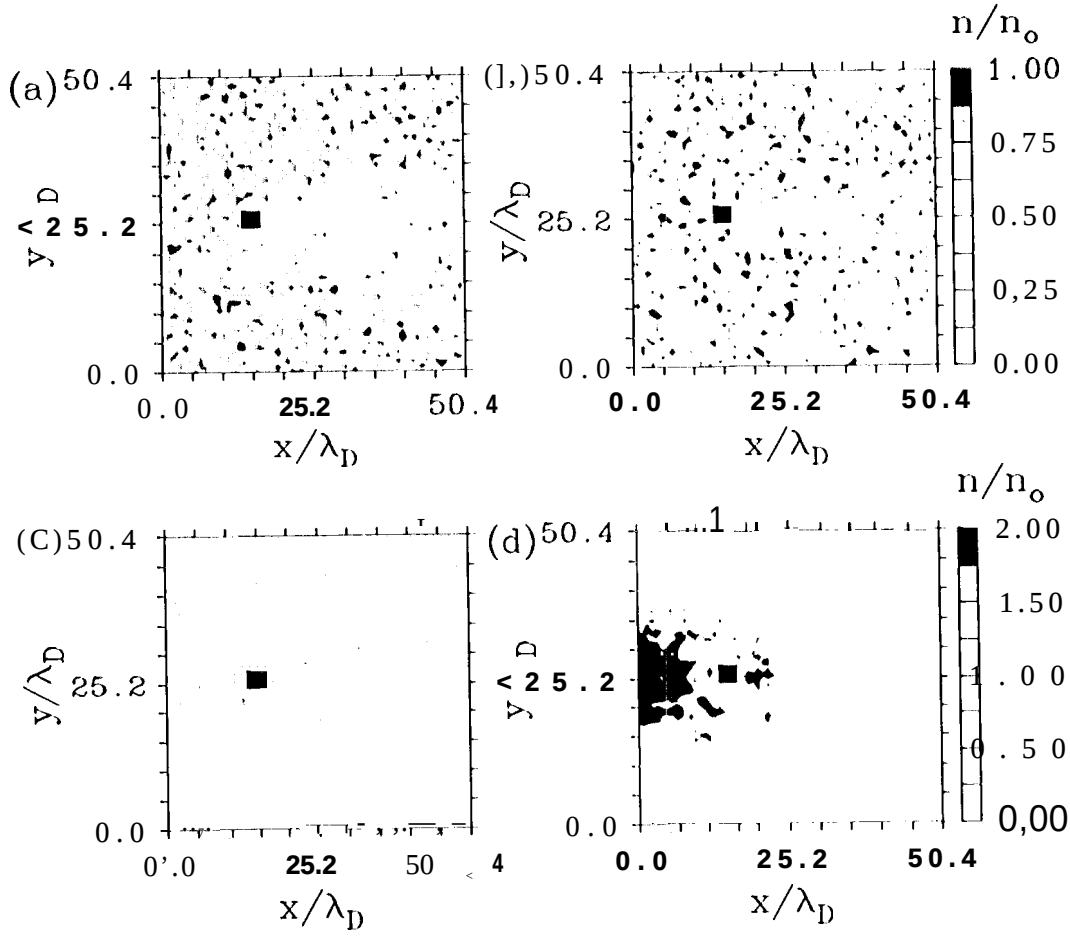

Figure **7:** The solar wind electron (a), proton (b), C_2 electron (c) and C_2 ion (d) density profiles for the case $\theta = 0^o$

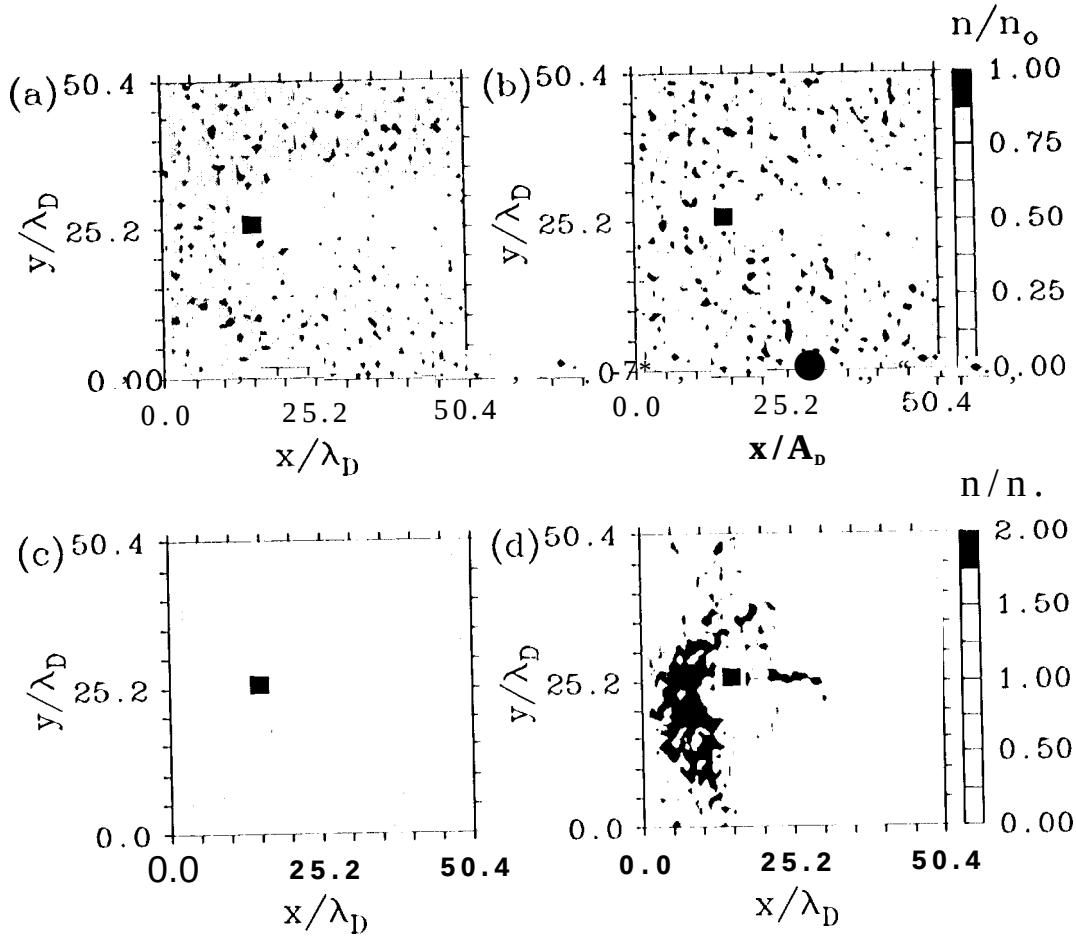

Figure 8: The solar wind electron (a), proton (1.)), C_2 electron (c) and C_2 ion (d) density profiles for the case O =- 300

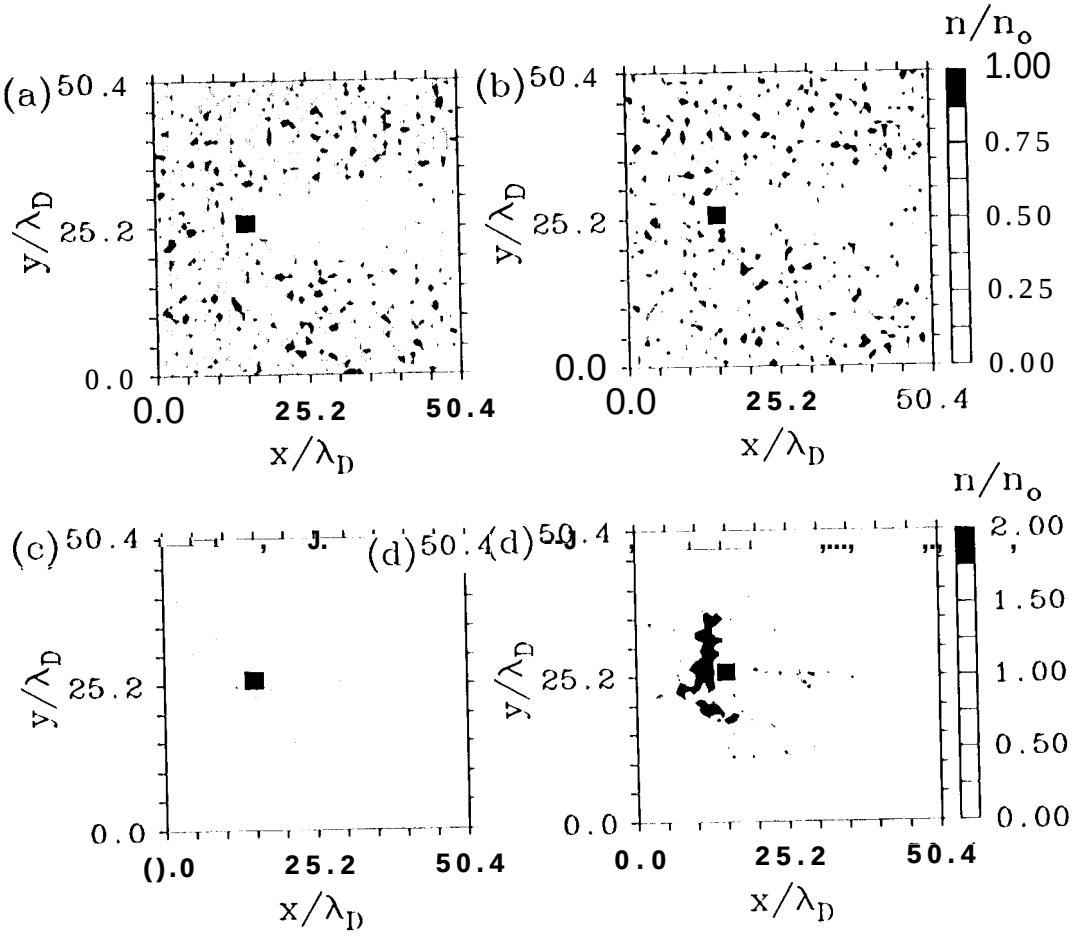

Figure 9: The solar wind electron (a), proton (b), C_2 electron (c) and C_2 ion (d) density profiles for the case $\theta = 90^o$.

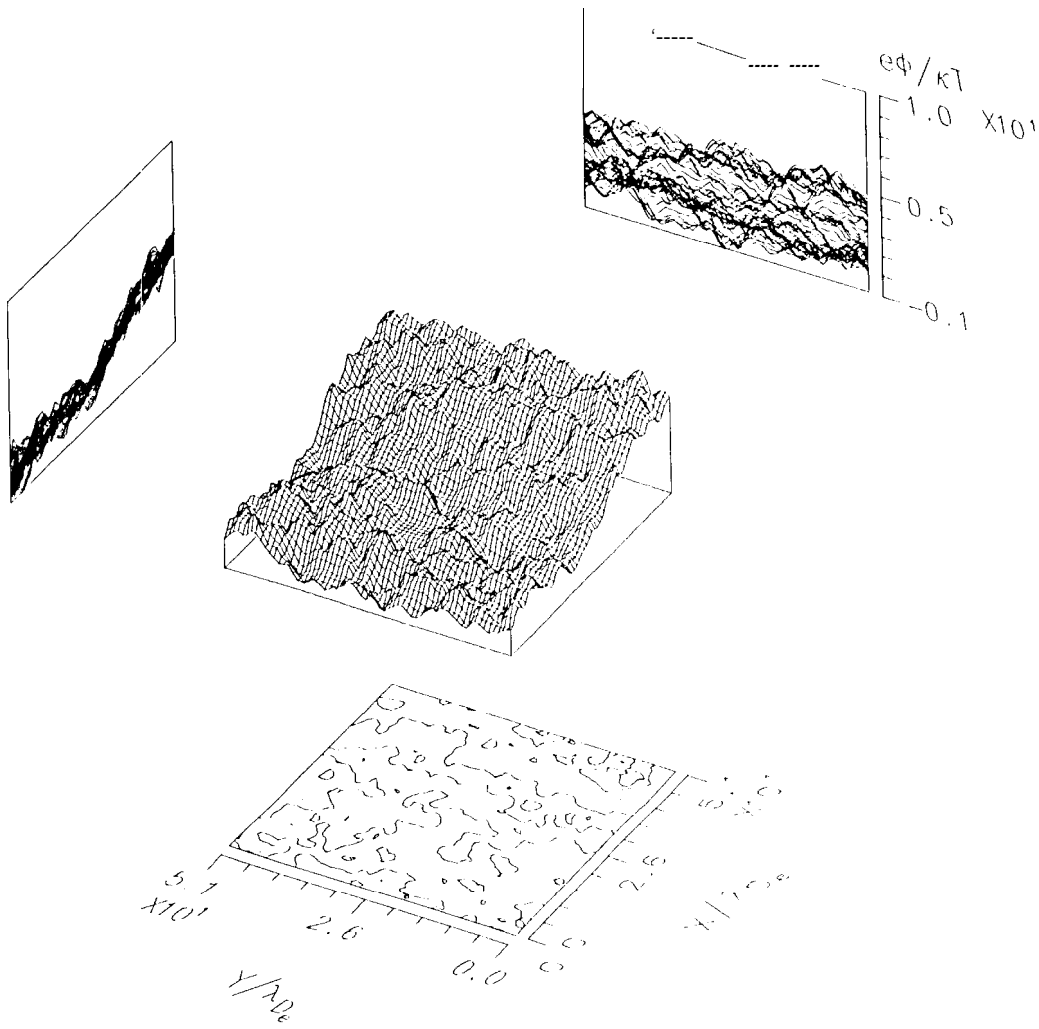

Figure 10: Potential structure in the vicinity of the spacecraft. Bottom panel depicts a contour map of the potential structure. Upper left and upper right figures show the projection of the potential structure onto the ϕ - x plane and ϕ - y plane, respectively. Potential energy $e\phi$ is normalized with the solar wind thermal energy $\kappa T \sim 1\ 00eV$,

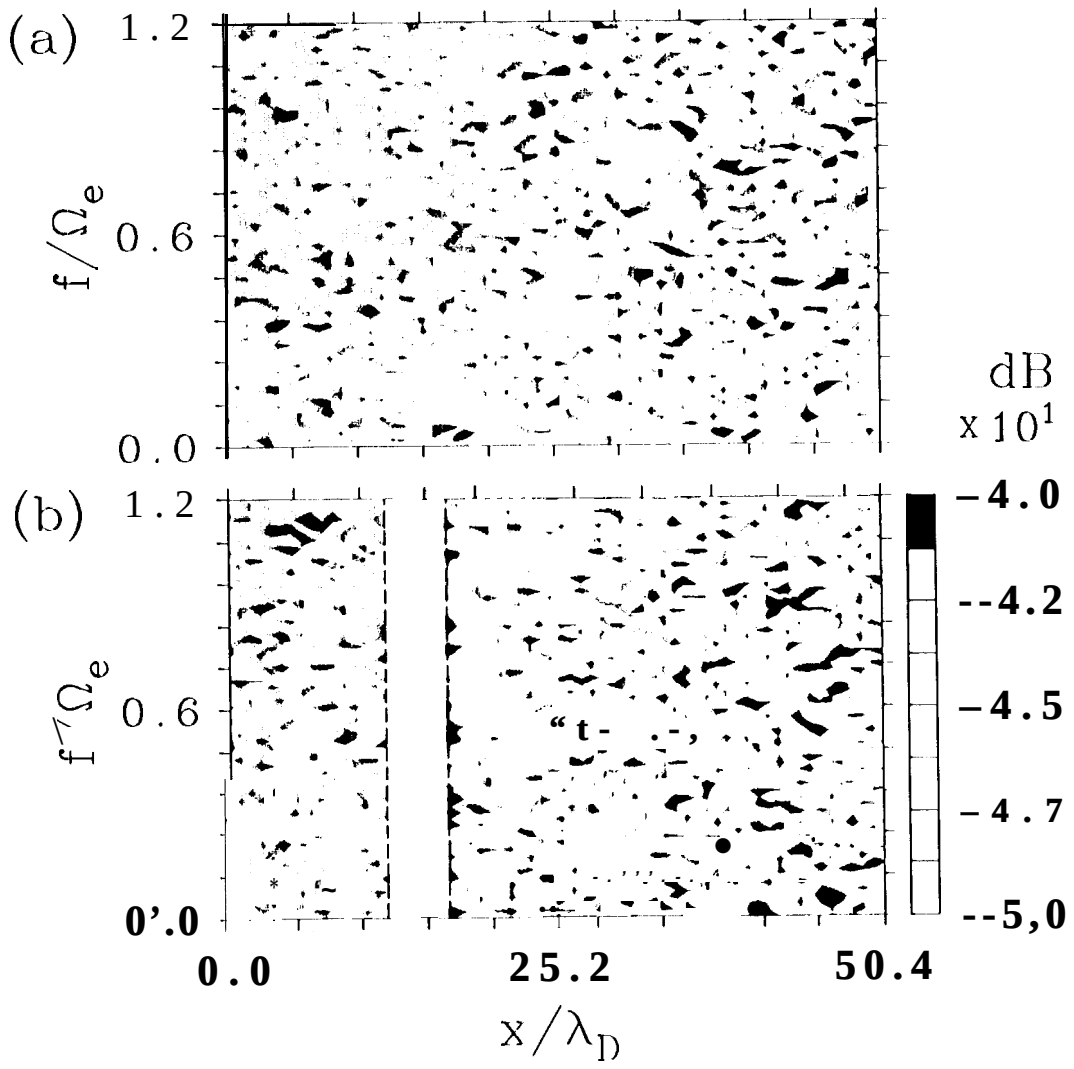

Figure 11: Frequency spectra of the electric field x component along the x axis at $y/\lambda_D =$ (a) 17.0 and (b) 25.2 when the C_2^+ plasma is present. $y/\lambda_D = 25.2$ corresponds to the location where the spacecraft is placed. The region delimited by dashed lines indicates the spacecraft location.

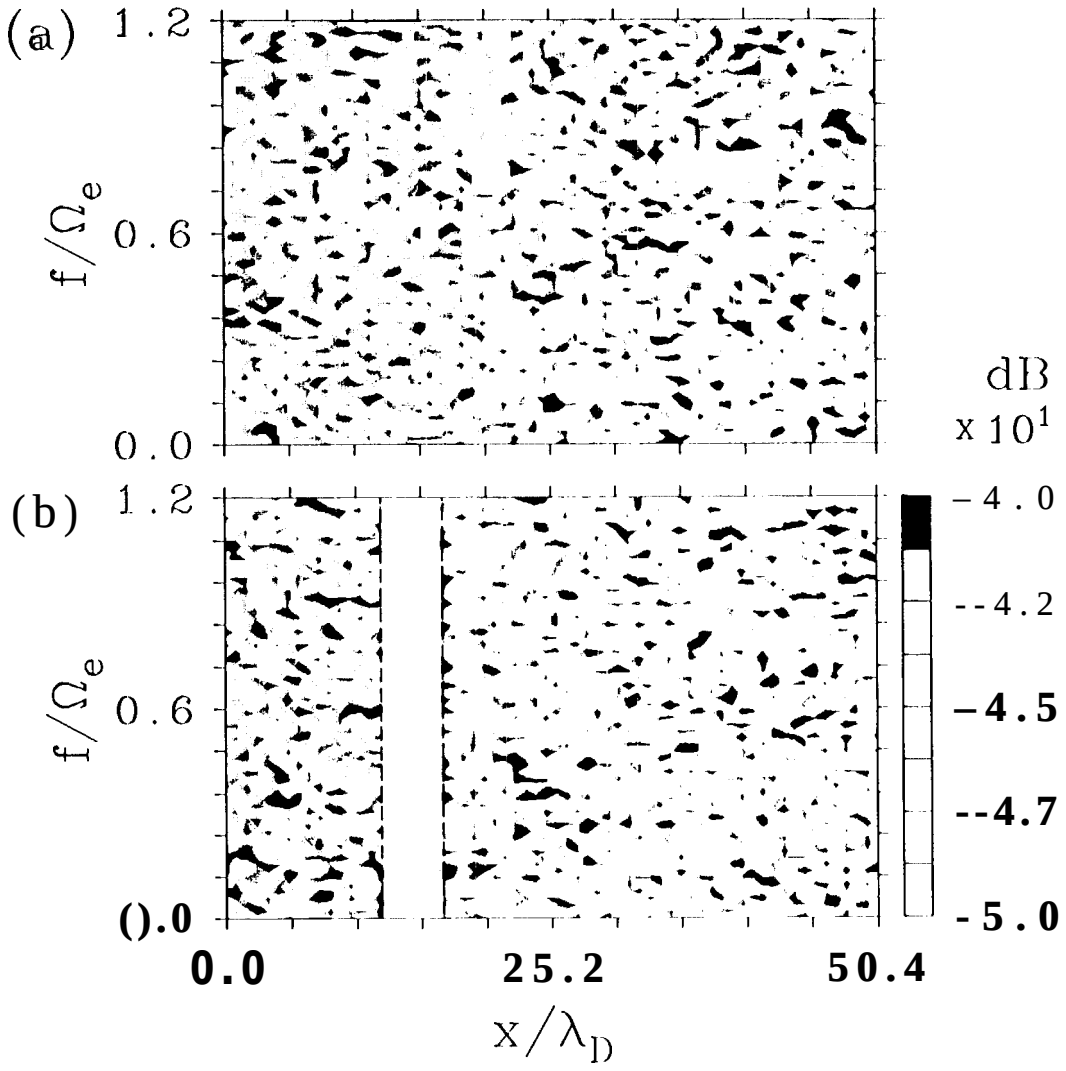

Figure 12: Frequency spectra of the electric field x component along the x axis at $y/\lambda_D =$ (a) 17.() and (b) 25.2 when the C_2^+ plasma is not present. $y/\lambda_D = 25.2$ corresponds to the location where the spacecraft is placed. The region delimited by dashed lines indicates the spacecraft location.